Reprinted from December, 1981, Vol. 48, Journal of Applied Mechanics

M. Y. He
Institute of Mechanics,
Chinese Academy of Sciences,
Beijing, China

J. W. Hutchinson
Division of Applied Sciences,
Harvard University,
Cambridge, Mass. 02138
Mem. ASME

The Penny-Shaped Crack and the Plane Strain Crack in an Infinite Body of Power-Law Material

A study is carried out of the problem of a penny-shaped crack in an infinite body of power-law material subject to general remote axisymmetric stressing conditions. The plane strain version of the problem is also examined. The material is incompressible and is characterized by small strain deformation theory with a pure power relation between stress and strain. The solutions presented also apply to power-law creeping materials and to a class of strain-rate sensitive hardening materials. Both numerical and analytical procedures are employed to obtain the main results. A perturbation solution obtained by expanding about the trivial state in which the stress is everywhere parallel to the crack leads to simple formulas which are highly accurate even when the remote stress is perpendicular to the crack.

1 Statement of Problems

Within the context of small strain theory we consider an incompressible, power-law solid characterized in simple tension by

$$\epsilon/\epsilon_0 = \alpha(\sigma/\sigma_0)^n \tag{1}$$

where ϵ_0 and σ_0 are a reference strain and stress and α is an extra constant introduced for convenience of application. For J_2 deformation theory, (1) generalizes to

$$\frac{\epsilon_{ij}}{\epsilon_0} = \frac{3}{2}\alpha\left(\frac{\sigma_e}{\sigma_0}\right)^{n-1}\frac{s_{ij}}{\sigma_0} \tag{2}$$

where s_{ij} is the stress deviator and σ_e is the effective stress defined by

$$\sigma_e = \left(\frac{3}{2}s_{ij}s_{ij}\right)^{1/2} \tag{3}$$

It is also convenient to define an effective strain

$$\epsilon_e = \left(\frac{2}{3}\epsilon_{ij}\epsilon_{ij}\right)^{1/2} \tag{4}$$

which coincides with the tensile strain in uniaxial tension so that σ_e and ϵ_e satisfy (1).

Two crack problems are analyzed below. The first is a penny-shaped crack of radius a subject to general remote axisymmetric stress conditions (see Fig. 1(a))

$$\sigma_{11}^{\infty} = \sigma_{33}^{\infty} = T, \quad \sigma_{22}^{\infty} = S \tag{5}$$

The second is the plane strain problem ($\epsilon_{33} = 0$) with a crack of half length a subject to inplane remote stresses (see Fig. 1(b))

$$\sigma_{11}^{\infty} = T, \quad \sigma_{22}^{\infty} = S \quad \left(\text{with } \sigma_{33}^{\infty} = \frac{1}{2}(S+T)\right) \tag{6}$$

In both problems the crack is traction-free. A number of fully plastic crack problems of this type have been analyzed [1–4], and an estimation scheme has been proposed for using these solutions together with linear elastic solutions to interpolate from small to large-scale yielding behavior [4–6].

The solutions presented as follows also apply to power-law creeping materials under steady-state creep conditions. The following pre-

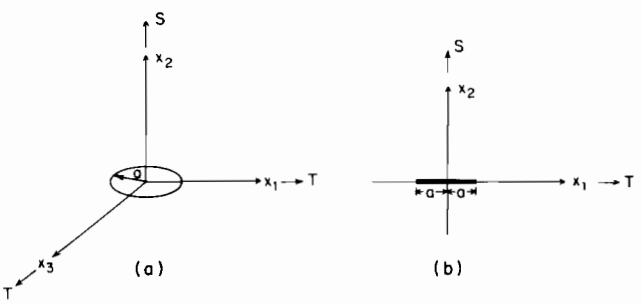

Fig. 1 Conventions: (a) penny-shaped crack, (b) plane strain crack

Contributed by the Applied Mechanics Division for publication in the JOURNAL OF APPLIED MECHANICS.
Discussion on this paper should be addressed to the Editorial Department, ASME, United Engineering Center, 345 East 47th Street, New York, N. Y. 10017, and will be accepted until two months after final publication of the paper itself in the JOURNAL OF APPLIED MECHANICS. Manuscript received by ASME Applied Mechanics Division, March, 1981.

sentation will use the time-independent formulation but conversion of the results to the steady creep interpretation is immediate. If S and T are increased (or decreased) monotonically in fixed proportion, the solution to the fully plastic crack problem has the property that the stress components also increase in fixed proportion at each point in the body. Consequently, the solutions are also exact solutions based on the J_2 flow (incremental) theory of plasticity fit to the same uniaxial relation (1), as discussed more fully in [1].

The fully plastic solutions can be used in addition to generate solutions to a class of strain-rate-dependent hardening solids [7, 8] which in simple tension satisfy

$$\sigma/\sigma_0 = \beta(\epsilon/\epsilon_0)^k(\dot{\epsilon}/\epsilon_0)^m \tag{7}$$

and for multiaxial states satisfy

$$\frac{s_{ij}}{\sigma_0} = \frac{2}{3}\beta\left(\frac{\epsilon_e}{\epsilon_0}\right)^{k-1}\left(\frac{\dot{\epsilon}_e}{\epsilon_0}\right)^m\frac{\epsilon_{ij}}{\epsilon_0} \tag{8}$$

where $(\dot{\ })$ here denotes the time rate of change. The solution to the fully plastic problem governed by (2) is of the form

$$u_i = \lambda\bar{u}_i, \quad \epsilon_{ij} = \lambda\bar{\epsilon}_{ij}, \quad \sigma_{ij} = \lambda^{1/n}\bar{\sigma}_{ij} \tag{9}$$

where λ is taken as a strain-based load parameter which is directly related to S and T. Spatial dependence is contained in the barred quantities. The corresponding solution to the strain-rate-dependent hardening problem governed by (8) in which the same load parameter varies with time according to $\lambda(t)$ is

$$u_i = \lambda\bar{u}_i, \quad \epsilon_{ij} = \lambda\bar{\epsilon}_{ij}, \quad \dot{\epsilon}_{ij} = \dot{\lambda}\bar{\epsilon}_{ij}, \quad \sigma_{ij} = \lambda^k\dot{\lambda}^m\bar{\sigma}_{ij} \tag{10}$$

where $k + m = 1/n$ and $\beta = (1/\alpha)^{1/n}$. The stressing is again proportional at each point in the body and, as long as λ varies such that σ_e does not decrease, the solution from (8) is as well a solution to the J_2 flow theory version of the constitutive law.

The family of power-law materials (2) includes an isotropic, incompressible linear elastic solid at one end of the range we will consider ($n = 1$) and a rigid-perfectly plastic solid with the yield condition $\sigma_e = \sigma_0$ at the other ($n = \infty$). The plane strain problem becomes hyperbolic with the possibility of discontinuous displacements across certain slip lines in the rigid-perfectly plastic limit. On the other hand, the axisymmetric problem for the penny-shaped crack is elliptic for all n including the limit $n = \infty$ so that discontinuities in strains and displacements are not possible. The differences in the characters of the two solutions for large n will be brought out in the following.

The outline of the paper is as follows. The theoretical background to the numerical solution is given in Section 2. The numerical method is described in Section 3 and results for the penny-shaped crack are then presented. A perturbation method is employed in Section 4 to generate solutions for remote stressing conditions departing only slightly from the trivial state in which $S = 0$ and $T \neq 0$. These relatively simple results are found to give highly accurate predictions even under remote tension conditions ($S > 0$, $T = 0$). The paper concludes with Section 5 in which numerical results for the plane strain problem are given.

2 Theoretical Background

Minimum Principle for Infinite Body. The displacement-based minimum principle for the infinite body given in [9] will be used. The principle is the standard minimum potential energy principle modified such that volume or area integrals remain bounded when applied to an infinite region. Let $\boldsymbol{\sigma}^\infty$, $\boldsymbol{\epsilon}^\infty$, and $\mathbf{u}^\infty$ denote the uniform fields associated with the uncracked body subject to prescribed S and T. Let an additional displacement field $\tilde{\mathbf{u}}$ be introduced such that the total displacement is

$$\mathbf{u} = \mathbf{u}^\infty + \tilde{\mathbf{u}} \tag{11}$$

where $u_{i,i} = u^\infty_{i,i} = \tilde{u}_{i,i} = 0$. With

$$\epsilon_{ij} = \frac{1}{2}(u_{i,j} + u_{j,i}) \quad \text{and} \quad \tilde{\epsilon}_{ij} = \frac{1}{2}(\tilde{u}_{i,j} + \tilde{u}_{j,i}) \tag{12}$$

the total strain is given by $\boldsymbol{\epsilon} = \boldsymbol{\epsilon}^\infty + \tilde{\boldsymbol{\epsilon}}$. It will be assumed that the additional displacement field decays faster than $r^{-1/2}$ as $r = (x_i x_i)^{1/2}$ becomes large. Then, among all admissible additional displacement fields satisfying this condition, the solution minimizes

$$\Phi(\tilde{\mathbf{u}}) = \int_V [W(\boldsymbol{\epsilon}) - W(\boldsymbol{\epsilon}^\infty) - \sigma^\infty_{ij}\tilde{\epsilon}_{ij}]dV - \int_S \sigma^\infty_{ij} n_j \tilde{u}_i dS \tag{13}$$

where V is the infinite region surrounding the crack, S is the crack surface, $\mathbf{n}$ is the unit normal to S pointing into V, and

$$W(\boldsymbol{\epsilon}) = \int_0^{\boldsymbol{\epsilon}} \sigma_{ij}d\epsilon_{ij} = \frac{n}{n+1}\alpha\sigma_0\epsilon_0\left(\frac{\epsilon_e}{\alpha\epsilon_0}\right)^{n+1/n} \tag{14}$$

Subject to the admissibility conditions on the decay of $\tilde{\mathbf{u}}$, the minimum principle holds in the limit $n = \infty$ with $\boldsymbol{\epsilon}^\infty \propto \mathbf{s}^\infty$ imposed and $\sigma^\infty_e = \sigma_0$. As will be discussed further, the condition on the decay of $\tilde{\mathbf{u}}$ is satisfied for the axisymmetric problem but not for the plane strain problem when $n = \infty$.

Relation Between Energy-Release Rate and $\Phi_{\min}$. Consider the penny-shaped crack centered in a solid sphere of material of radius R (which will subsequently be permitted to become unbounded) and let tractions $T^\infty_i \equiv \sigma^\infty_{ij} n_j$ be imposed on the outer surface S_R of the sphere. (For the plane strain problem the crack is taken to be centered in a cylinder of radius R, but otherwise the argument which follows applies to plane strain as well.) The potential energy of the cracked body V_R subject to $\mathbf{T}^\infty$ on S_R is

$$PE(a) = \int_{V_R} W(\boldsymbol{\epsilon})dV - \int_{S_R} T^\infty_i u_i\, dS \tag{15}$$

For an increase of radius of the crack from a to $a + da$ with $\mathbf{T}^\infty$ held fixed, the energy-release rate per unit length of crack edge is

$$J = -\frac{1}{2\pi a}\frac{dPE}{da} \tag{16}$$

Next, we show that $dPE/da = d\Phi_{\min}/da$ when $R \to \infty$. By the principle of virtual work

$$\int_{S_R} T^\infty_i \tilde{u}_i dS = \int_{V_R} \sigma^\infty_{ij}\tilde{\epsilon}_{ij}\, dV + \int_S \sigma^\infty_{ij} n_j \tilde{u}_i dS \tag{17}$$

where $\tilde{\mathbf{u}}$ is the additional displacement defined in (11) and on the surface of the crack, S, the unit normal $\mathbf{n}$ points into V_R. Use (17) to rewrite (15) as

$$PE(a) = \int_{V_R} [W(\boldsymbol{\epsilon}) - W(\boldsymbol{\epsilon}^\infty) - \sigma^\infty_{ij}\tilde{\epsilon}_{ij}]dV - \int_S \sigma^\infty_{ij} n_j \tilde{u}_i dS + C \tag{18}$$

where the terms comprising C depend only on the uniform state $\boldsymbol{\sigma}^\infty$ and are independent of a. Subject to the same decay conditions on $\tilde{\mathbf{u}}$ required for the minimum principle, $PE - C$ becomes $\Phi_{\min}$ as R becomes unbounded and therefore

$$dPE/da = d\Phi_{\min}/da \tag{19}$$

By dimensional considerations $\Phi_{\min}$ must have the functional form

$$\Phi_{\min} = \sigma_0\epsilon_0 a^3 f(n, S/T, S/\sigma_0) \tag{20}$$

and thus

$$d\Phi_{\min}/da = 3\sigma_0\epsilon_0 a^2 f = 3\Phi_{\min}/a \tag{21}$$

It follows then from (16), (19), and (21) that

$$J = -\frac{3}{2\pi a^2}\Phi_{\min} \tag{22}$$

For any admissible additional displacement field $\tilde{\mathbf{u}}$, $\Phi(\tilde{\mathbf{u}}) \geq \Phi_{\min}$ and thus an estimate of J using

$$J = -\frac{3}{2\pi a^2}\Phi(\tilde{\mathbf{u}}) \tag{23}$$

is necessarily a *lower bound*. Equation (23) will be used to obtain our numerical estimates of J.

For the plane strain crack (16), (20), and (22) are replaced by, respectively,

$$J = -\frac{1}{2}\frac{dPE}{da} \tag{24}$$

$$\Phi_{\min} = \sigma_0 \epsilon_0 a^2 f(n, S/T, S/\sigma_0) \tag{25}$$

$$J = -\Phi_{\min}/a \tag{26}$$

Analogous relations based on a modified complementary potential energy functional can also be formulated. For statically admissible stress fields, the complementary formulation generates upper bound estimates of J. This alternative approach has not been used here. In [3], both of the unmodified minimum principles have been used to produce numerical estimates of J for problems involving cracks in finite geometries. The numerical results in [3] do appear to provide the corresponding lower and upper bounds, even though it is unlikely that the strict bounding properties, which hold for the infinite body, apply to finite geometries.

Crack-Tip Fields and the Relation Between J and the M-Integral for the Penny-Shaped Crack. For the plane strain problem J as defined here is equal to the line integral definition of J [10]. The singular crack-tip fields are of the form

$$\sigma_{ij} = \sigma_0 \left(\frac{J}{\alpha \sigma_0 \epsilon_0 I_n r}\right)^{1/n+1} \tilde{\sigma}_{ij}(\theta, n), \quad \epsilon_{ij} = \alpha \epsilon_0 \left(\frac{J}{\alpha \sigma_0 \epsilon_0 I_n r}\right)^{n/n+1} \tilde{\epsilon}_{ij}(\theta, n) \tag{27}$$

where (r, θ) are planar polar coordinates centered at the crack tip and where details of the θ-variations and the normalizing constant I_n are given in [11, 12].

The plane strain singular fields (27) also hold at the edge of a penny-shaped crack, where r and θ are then local coordinates in a plane perpendicular to the edge of the crack. Because the circumferential strain is bounded at the crack edge, the singular field is necessarily a plane strain field with the same functional dependence on r and θ as in (27). The easiest way to see that J, which has been defined here as the energy-release rate in (16), is the amplitude of the singular fields in (27) is to invoke a surface-independent integral [13] called the M-integral in [14]. For the power-law material (2),

$$M = \int_S \left[W x_i n_i - \sigma_{ij} n_j u_{i,k} x_k - \left(\frac{2n-1}{n+1}\right) \sigma_{ij} n_j u_i \right] dS \tag{28}$$

where S is any closed surface which encloses the crack and $\mathbf{n}$ is the unit outward normal to S at each point. In [14] it is shown that M/a is the total energy-release rate with respect to a. Thus, for our definition of J in (16), it follows that

$$J = M/(2\pi a^2) \tag{29}$$

Now deform the surface S in (28) to a torus-like surface ringing the edge of the penny-shaped crack. (The integrand vanishes on the faces of the crack.) As the torus is shrunk down to the edge of the crack, only the singular terms in the integrand of (28) contribute to M, and it is readily seen that $M/(2\pi a^2)$ is just the line-integral definition of J for plane strain. This establishes that J as defined in (16) for the penny-shaped crack is indeed the amplitude of the singular crack-tip fields as it appears in (27).

3 Numerical Solution for Penny-Shaped Crack

A numerical procedure based on the approximate minimization of Φ in (13) as developed in [9, 15] will be employed. A stream function $\psi(x, y)$ is used to generate the additional axisymmetric displacements according to

$$\tilde{u}_x = x^{-1}\psi_{,y} \quad \text{and} \quad \tilde{u}_y = -x^{-1}\psi_{,x} \tag{30}$$

where x and y are radial and axial cylindrical coordinates (which coincide with x_1 and x_2, respectively, in the trace plane $x_3 = 0$) and $\tilde{u}_x$ and $\tilde{u}_y$ are the associated additional displacements.

To expedite numerical integration the region outside the crack in the trace plane $x_3 = 0$ is mapped onto the interior of the unit circle in the ζ-plane (see Fig. 2) using

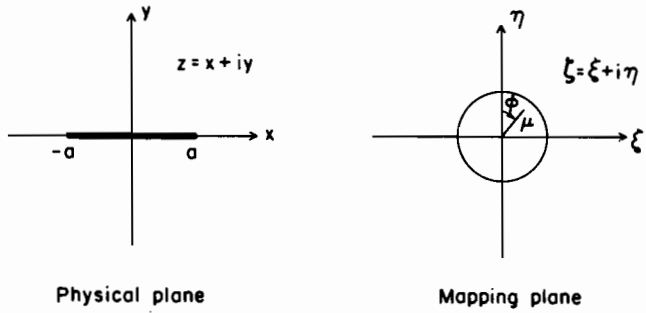

Fig. 2 Mapping of physical trace plane onto interior of the unit circle in the ζ-plane

$$z \equiv x + iy = \omega(\zeta) = \frac{a}{2}(\zeta + \zeta^{-1}) \quad (i = \sqrt{-1}) \tag{31}$$

With μ and ϕ as planar-polar coordinates in the mapping plane as shown in Fig. 2 and with ψ regarded as a function of these coordinates,

$$\tilde{u}_x = \frac{1}{x}\left(\psi_{,\mu}\frac{\partial \mu}{\partial y} + \psi_{,\phi}\frac{\partial \phi}{\partial y}\right), \quad \tilde{u}_y = -\frac{1}{x}\left(\psi_{,\mu}\frac{\partial \mu}{\partial x} + \psi_{,\phi}\frac{\partial \phi}{\partial x}\right) \tag{32}$$

where, with $\Omega = \zeta(d\omega/d\zeta)$,

$$\frac{\partial \mu}{\partial x} + i\frac{\partial \mu}{\partial y} = \mu\frac{\Omega}{|\Omega|^2}, \quad \frac{\partial \phi}{\partial y} - i\frac{\partial \phi}{\partial x} = -\frac{\Omega}{|\Omega|^2} \tag{33}$$

Expressions for the additional strain components from $\psi(\mu, \phi)$ are given in the Appendix.

An approximate representation of the stream function is taken as

$$\psi(\mu, \phi) = F(\mu, \phi)\left[A_0 + \sum_{k=1}^{N}\sum_{j=0}^{M} A_{kj}\mu^j \mu_k(\phi)\right] \tag{34}$$

where

$$F(\mu, \phi) = (1 - \mu^\beta \sin^2\phi)\cos\phi \tag{35}$$

The A's and β are treated as variables in the minimization of Φ. In terms of the polar mapping coordinates, $\mu = 1$ corresponds to the crack surface while $\mu \to 0$ corresponds to $x^2 + y^2 \to \infty$. The range of ϕ is from 0 to π with ψ being symmetric in ϕ about $\phi = \pi/2$. The choice of F in (34) and (35) insures a uniform representation leading to admissible behavior at the poles and a smooth opening of the crack, as will be discussed later. The terms in the square brackets in (34) are derived from a complete double series which has been truncated consistent with admissibility conditions. These require that u_k is symmetric about $\phi = \pi/2$ and that $u_k(0) = u_k'(0) = 0$. The set of orthogonal eigenfunctions used for the ϕ-variation in (34) is

$$u_k(\phi) = \cos\lambda_k\left(\phi - \frac{\pi}{2}\right) + b_k \cosh\lambda_k\left(\phi - \frac{\pi}{2}\right) \tag{36}$$

where the λ_k satisfy

$$\cos\left(\frac{\lambda_k\pi}{2}\right)\sinh\left(\frac{\lambda_k\pi}{2}\right) + \sin\left(\frac{\lambda_k\pi}{2}\right)\cosh\left(\frac{\lambda_k\pi}{2}\right) = 0 \tag{37}$$

and

$$b_k = \sin\left(\frac{\lambda_k\pi}{2}\right)/\sinh\left(\frac{\lambda_k\pi}{2}\right) \tag{38}$$

The first four λ_k and b_k are

$$\begin{aligned} \lambda_1 &= 1.5056187 & b_1 &= 0.1328565 \\ \lambda_2 &= 3.5000107 & b_2 &= -5.792274 \times 10^{-3} \\ \lambda_3 &= 5.5000000 & b_3 &= 2.503110 \times 10^{-4} \\ \lambda_4 &= 7.5000000 & b_4 &= -1.08169 \times 10^{-5} \end{aligned} \tag{39}$$

With $\psi = A_0 F(\mu, \phi)$, the crack opening displacement $\delta(x) = u_y(x, 0^+) - u_y(x, 0^-)$ is

Table 1 h_1, h_2, and h_3 for penny-shaped crack

$h_1(n, S/T)$

S/σ_e^∞	S/T	n = 1	n = 1.5	n = 2	n = 3	n = 5	n = 10	n = ∞
1	∞	0.9549	1.094	1.194	1.331	1.484	1.639	1.841
2	2.0	3.819	4.372	4.758	5.248	5.734	6.141	6.669
3	1.50	8.594	10.05	11.12	12.55	14.12	15.75	18.24
4	1.33	15.28	18.59	21.23	25.30	31.03	39.13	55.65
5	1.25	23.87	30.45	36.35	47.09	65.42		
0.5	-1.0	0.2387	0.2736	0.2978	0.3297	0.3641	0.3983	0.4448
0.2	-0.25	0.03819	0.04386	0.04774	0.05279	0.05815	0.06338	0.07030
0.1	-0.111	0.009549	0.01097	0.01195	0.01320	0.01453	0.01581	0.01748

$h_2(n, S/T)$

S/σ_e^∞	S/T	n = 1	n = 1.5	n = 2	n = 3	n = 5	n = 10	n = ∞
1	∞	4.000	4.575	4.992	5.554	6.159	6.709	7.270
2	2.0	8.000	9.232	10.08	11.17	12.41	12.83	14.90
3	1.5	12.00	14.74	16.92	19.99	23.78	28.83	38.96
4	1.33	16.00	21.19	25.94	34.83	50.29	75.96	130.6
5	1.25	20.00	28.64	37.87	57.77	97.52		
0.5	-1.0	2.000	2.289	2.492	2.761	3.053	3.347	3.749
0.2	-0.25	0.8000	0.9179	0.9992	1.105	1.219	1.330	1.480
0.1	-0.111	0.4000	0.4594	0.5002	0.5529	0.6087	0.6631	0.7342

$$\delta(x) = \frac{6}{a^3} A_0 \sqrt{a^2 - x^2} \tag{40}$$

Contributions from the other terms in (34) result in an opening displacement of the form $f(x)\sqrt{a^2 - x^2}$ where f is bounded at $x = a$. Thus (34) only contains the correct behavior for δ as $x \to a$ for the case $n = 1$. For $n > 1$, (34) can only approximate the correct behavior (i.e., $\delta \propto (a - x)^{1/n+1}$). In the neighborhood of the crack edge ($\mu = 1, \phi \approx \pi/2$)

$$\tilde{u}_x \cong -\frac{\beta}{3\left(\frac{\pi}{2} - \phi\right)} u_y \cong -\frac{\beta}{4}\left[A_0 + \sum_{k=1}^{N}\sum_{j=0}^{M} A_{kj}(1 + b_k)\right] \tag{41}$$

By allowing β to be a free variable in the minimization process, we remove the constraint between $\tilde{u}_x$ and u_y implied by (41) when β is fixed. (For $n = 1$, β turns out to be essentially zero and is always less in magnitude than 0.3.)

The surface integral contribution to Φ in (13) when evaluated using the representation (34) is just

$$-\int_S \sigma_{ij}^\infty n_j \tilde{u}_i \, dS = 4\pi \, \sigma_{22}^\infty A_0 \tag{42}$$

In terms of the coordinate variables μ and ϕ, the volume integral in (13) becomes an iterated double integral with the ranges $0 \le \mu \le 1$ and $0 \le \phi \le \pi/2$. For given numerical values of β and the A's, this integral is evaluated using an iterated application of a 10-point Gaussian integration formula. Minimization of Φ with respect to a given set of the free variables, β and the A's, is achieved using a numerically implemented Newton-Raphson method, which is described in more detail in [9]. For given numerical values of the free variables the volume integral in (13) is accurate to at least four significant figures. Thus the lower bound character of our estimates of J is preserved to this level of accuracy.

The functional form of the solution is

$$\begin{aligned} \frac{J}{\sigma_e^\infty \epsilon_e^\infty a} &= h_1\left(n, \frac{S}{T}\right) \\ \frac{\Delta V}{\epsilon_e^\infty a^3} &= h_2\left(n, \frac{S}{T}\right) \\ \frac{\delta}{\epsilon_e^\infty a} &= h_3\left(n, \frac{S}{T}\right) \end{aligned} \tag{43}$$

where ΔV is the volume of the opened crack and $\delta = u_y(0,0^+) - u_y(0,0^-)$ is opening of the crack at its center. For the axisymmetric problem

$$\sigma_e^\infty = |S - T| \tag{44}$$

and ϵ_e^∞ is related to σ_e^∞ by (1). Numerical results for h_1, h_2, and h_3 for various S/T and n are given in Table 1.

An indication of the convergence of the lower bound estimates of h_1 as dependent on the number of free parameters in (34) can be seen in Table 2 for the case of remote uniaxial tension ($S > 0$, $T = 0$). For the linear problem ($n = 1$) only 5 free parameters are required to give h_1 exactly to four significant figures. For the rigid-perfectly plastic problem ($n = \infty$) the convergence is slower with a 5 percent difference between the calculation with ($N = 2, M = 3$) and that with ($N = 3, M = 3$). The results in Table 1 for the case of remote uniaxial tension were determined with ($N = 3, M = 3$) for a total of 11 free parameters. The other results were obtained with ($N = 2, M = 3$) for a total of 8 free parameters.

Plots of the normalized J and ΔV as functions of the ratio S/σ_e^∞ are given in Figs. 3 and 4. With $\sigma_m^\infty = (S + 2T)/3$ as the remote mean stress, remote triaxiality is measured by

$$\frac{\sigma_m^\infty}{\sigma_e^\infty} = \frac{S}{\sigma_e^\infty} - \frac{2}{3}$$

for $S - T > 0$. The very strong dependence of ΔV on triaxiality for

Table 1 (Continued)

$h_3(n, S/T)$

S/σ_e^∞	S/T	n = 1.0	n = 1.5	n = 2.0	n = 3.0	n = 5.0	n = 10	n = ∞
1	∞	1.909	2.093	2.218	2.375	2.525	2.637	2.690
2	2.0	3.818	4.069	4.226	4.415	4.671	4.753	5.358
3	1.5	5.727	6.496	7.059	7.760	8.595	9.812	12.30
4	1.333	7.637	9.395	10.92	13.85	19.16	28.27	47.75
5	1.250	9.546	12.79	16.23	23.92	40.07		
0.5	-1.0	0.9546	1.091	1.183	1.320	1.426	1.545	1.698
0.2	-0.25	0.3824	0.4428	0.4852	0.5405	0.5996	0.6570	0.7329
0.1	-0.111	1.910	0.2224	0.2445	0.2734	0.3045	0.3348	0.3746

Table 2 h_1 for different numbers of free parameters ($S > 0$, $T = 0$)

	N = 1, M = 3	N = 2, M = 2	N = 2, M = 3	N = 3, M = 3
n = 1.0	0.9549	0.9549	0.9549	0.9549
n = 1.5	1.089	1.090	1.092	1.094
n = 5	1.423	1.432	1.453	1.484
n = ∞	1.680	1.716	1.756	1.841

$\sigma_m^\infty/\sigma_e^\infty$ above unity when n is 3 or greater is similar to the dependence of the dilatation of a spherical void on triaxiality [9, 16].

The profile of the opened crack is shown in Fig. 5 for several n-values for the case of remote uniaxial tension ($S > 0$, $T = 0$; or $S/\sigma_e^\infty = 1$). Contours on which the effective strain is a constant are shown in Fig. 6 for $n = 5$ and in Fig. 7 for $n = \infty$, both for the case of remote uniaxial tension and both with $\epsilon_e^\infty = 1$.

4 Perturbation Solution

Penny-Shaped Crack. The uniform state $\sigma_{22} = 0$, $\sigma_{11} = \sigma_{33} = T$ is a trivial solution to the penny-shaped crack problem. In this section we develop an exact perturbation solution about this state. For the linear problem ($n = 1$) nothing new will be learned from this solution. However, for the nonlinear problems ($n \neq 1$) we will obtain relatively simple results which not only hold for remote stressing conditions slightly perturbed from the trivial state but also for remote uniaxial tension with a fairly high degree of accuracy.

In the uniform trivial state ($S = 0$, $T < 0$) the crack remains closed, J is zero and the nonzero strain components from (2) are

$$\epsilon_{22} = -2\epsilon_{11} = -2\epsilon_{33} = \epsilon_e = \alpha\epsilon_0(|T|/\sigma_0)^n \tag{45}$$

Onto this trivial state we superimpose an increment of remote tensile stress $\dot{\sigma}^\infty$ parallel to the x_2-axis and perpendicular to the traction-free crack so that

$$\sigma_{22}^\infty \equiv S = \dot{\sigma}^\infty \quad \text{and} \quad \sigma_{11}^\infty = \sigma_{33}^\infty \equiv T \tag{46}$$

From (2), the increments in deviatoric stress and strain throughout the body satisfy

$$\dot{s}_{ij} = L_{ijkl}\dot{\epsilon}_{kl} \quad (\dot{\epsilon}_{kk} = 0) \tag{47}$$

where the incremental moduli are

$$L_{ijkl} = 2\mu\left\{\frac{1}{2}(\delta_{ik}\delta_{jl} + \delta_{il}\delta_{jk}) - \frac{1}{3}\delta_{ij}\delta_{kl} + \frac{2}{3}\frac{(1-n)}{n}\epsilon_{ij}\epsilon_{kl}\epsilon_e^{-2}\right\} \tag{48}$$

with

$$\mu = \frac{1}{3}\frac{\sigma_e}{\epsilon_e} \tag{49}$$

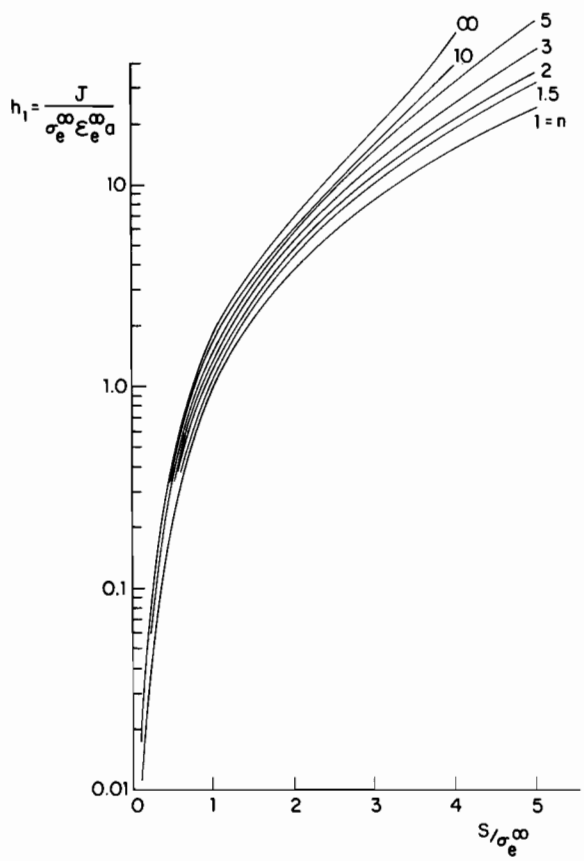

Fig. 3 Normalized J for penny-shaped crack

The incremental problem is a standard linear elastic crack problem for an incompressible material with uniform moduli (48) which are transversely isotropic with respect to the x_2-axis. The solution to this problem has been given in the literature but we have had some difficulty in gleaning the information desired here from published studies. In what follows, we sketch out the details for obtaining J, ΔV, and δ for the present incremental problem following for the most part a solution procedure used in [17] for the more general problem of an elliptical crack in a linear anisotropic solid. In this section it is important not to lose sight of the fact that it is the *linear incremental problem* which is being analyzed. When $S \neq 0$ it is always possible to find a zone sufficiently near the tip where the perturbation breaks down regardless of how small S is. Nevertheless, the perturbation solution does provide a rigorous expansion of J and ΔV for small S.

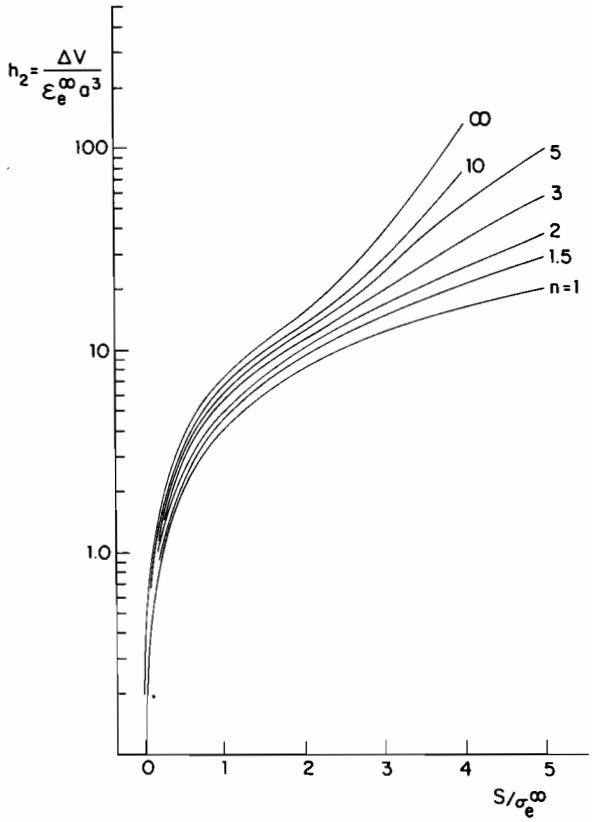

Fig. 4 Normalized volume of opened penny-shaped crack

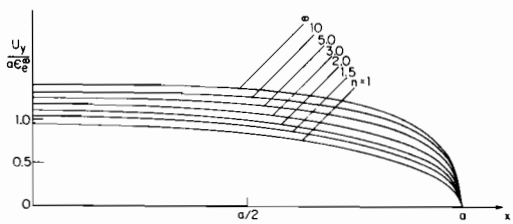

Fig. 5 Crack opening displacements for penny-shaped crack subject to remote uniaxial tension

In addition, the expansion of the crack opening displacement at any fixed point away from the tip is asymptotically correct as S approaches zero.

From the fundamental work on the general ellipsoidal inclusion problems [18] it is known that an elliptical crack in a homogeneous linear elastic solid opens into an ellipsoid. In the present incremental problem for the penny-shaped crack, both the moduli and the loading preserve axial symmetry about the x_2-axis and thus the opening of the crack is necessarily given by

$$\delta(R) = c(\dot{\sigma}^\infty/\mu)\,(a^2 - R^2)^{1/2} \tag{50}$$

where R is the distance from the center of the crack in its plane and c is an unknown dimensionless factor which, by dimensional analysis, depends only on n. The volume of the opened crack is

$$\Delta V = 2\pi \int_0^a \delta(R) R dR = \frac{2\pi}{3} c(\dot{\sigma}^\infty/\mu) a^3 \tag{51}$$

Next, consider the total energy released by creating a crack of radius a in a linear solid subject to a remote stress $\dot{\sigma}^\infty$ for which the opening displacement is (50); it is

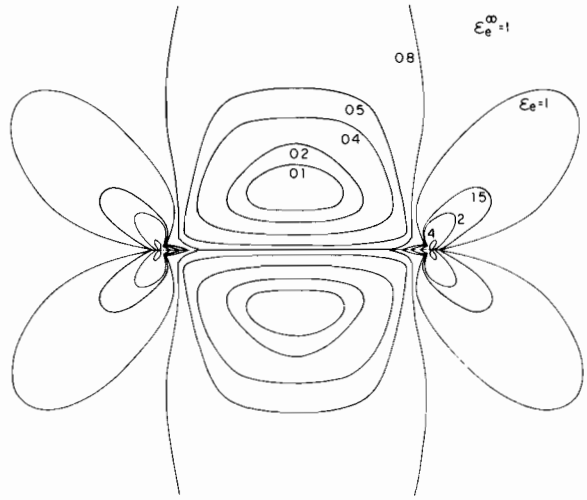

Fig. 6 Contours of constant effective strain ϵ_e for penny-shaped crack subject to remote uniaxial tension with $\epsilon_e^\infty = 1$ for $n = 5$

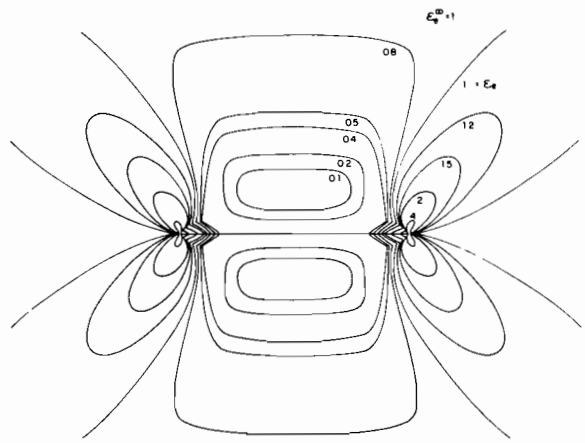

Fig. 7 Contours of constant effective strain ϵ_e for penny-shaped crack subject to remote uniaxial tension with $\epsilon_e^\infty = 1$ for $n = \infty$

$$E = \frac{1}{2} 2\pi \int_0^a \delta(R)\dot{\sigma}^\infty R dR = \frac{1}{2}\dot{\sigma}^\infty \Delta V \tag{52}$$

With J as the energy-release rate per unit length of crack edge, as defined earlier, it follows from (51) and (52) that

$$J = \frac{1}{2\pi a}\frac{dE}{da} = \frac{c}{2\mu}(\dot{\sigma}^\infty)^2 a \tag{53}$$

Another independent expression for J can be obtained by calculating the work done by the singular stresses at the crack edge through the crack opening for an incremental advance of the crack with $\dot{\sigma}^\infty$ held constant, i.e.,

$$J = \lim_{\Delta a \to 0} \frac{1}{2\Delta a} \int_0^{\Delta a} \dot{\sigma}_{22}(\xi, a)\delta(\xi, a + \Delta a) d\xi \tag{54}$$

where $\xi = R - a$. Here $\dot{\sigma}_{22}(\xi,a)$ denotes the stress acting at $R = a + \xi$ on the plane of the crack $x_2 = 0$ when the crack has radius a, and $\delta(\xi, a + \Delta a)$ is the crack opening at the same point associated with a crack of radius $a + \Delta a$. The singularity of $\dot{\sigma}_{22}$ at the crack edge necessarily has the form

$$\dot{\sigma}_{22} = \frac{k\dot{\sigma}^\infty \sqrt{a}}{\sqrt{2\pi\xi}} \tag{55}$$

for the incremental problem where k can only depend on n. Performing the calculation in (54) using (50) and (55), we find

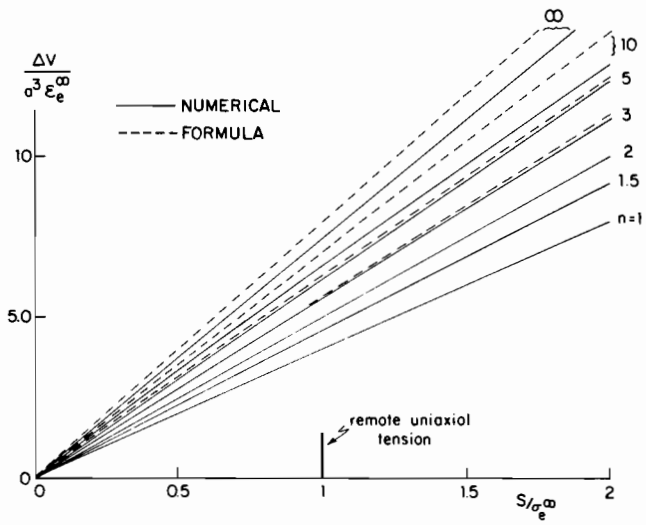

Fig. 8 Comparison between analytical results (84) and numerical results for penny-shaped crack

$$J = \frac{\sqrt{\pi}}{4}\frac{ck}{\mu}(\dot{\sigma}^{\infty})^2 a \tag{56}$$

By comparing (56) with (53) we see immediately that $k = 2/\sqrt{\pi}$, giving the classical result for a penny-shaped crack in an isotropic material. Thus the stress singularity on the plane of the crack is independent of n, i.e., independent of the degree of transverse anisotropy for this class of incremental, incompressible problems.

It remains to determine c. This is achieved by carrying out a local singularity analysis at the edge of the crack and then reconciling the result with (50) and (55). The singularity field at the edge of the penny-shaped crack is a plane strain field. Let ξ and η be local Cartesian coordinates in the plane $x_3 = 0$ with origin at the crack edge and parallel to the x_1 and x_2 axes, respectively. For the singularity field in the local coordinates, $\dot{\epsilon}_{33} = 0$ and $\dot{\epsilon}_{11} + \dot{\epsilon}_{22} = 0$. The latter constraint implies the existence of a stream function $\psi(\xi,\eta)$ such that $\dot{u}_1 = \psi_{,\eta}$ and $\dot{u}_2 = -\psi_{,\xi}$. Incremental equilibrium requires

$$\psi_{,\xi\xi\xi\xi} + \left(\frac{3}{n} - 1\right)\psi_{,\xi\xi\eta\eta} + \psi_{,\eta\eta\eta\eta} = 0 \tag{57}$$

where (48) has been used to express the stresses in terms of ψ in the equilibrium equations. Traction-free conditions on the crack flanks require

$$\left.\begin{aligned}\psi_{,\xi\xi} - \psi_{,\eta\eta} &= 0\\ 3\psi_{,\xi\xi\eta} + n\psi_{,\eta\eta\eta} &= 0\end{aligned}\right\}\ (\xi < 0, \eta = \pm 0) \tag{58}$$

Only the pertinent details of the singularity field solution of (57) and (58) will be given here. These are

$$\dot{\sigma}_{22} = A\xi^{-1/2} \quad (\xi > 0, \eta = 0) \tag{59}$$

and

$$\delta = \dot{u}_2(\xi, 0^+) - \dot{u}_2(\xi, 0^-) = \frac{4}{\mu}\left(1 + \frac{3}{n}\right)^{-1/2} A(-\xi)^{1/2} \quad (\xi < 0) \tag{60}$$

where A is an amplitude factor which is undetermined by the singularity analysis. Equations (59) and (55) (with $k = 2/\sqrt{\pi}$) imply

$$A = \dot{\sigma}^{\infty}(2a)^{1/2}/\pi \tag{61}$$

Near the edge of the crack (50) becomes $\delta = c(\dot{\sigma}^{\infty}/\mu)(-2a\xi)^{1/2}$; thus from (60) and (61) we find

$$c = \frac{4}{\pi}\left(1 + \frac{3}{n}\right)^{-1/2} \tag{62}$$

To further reduce the expressions for ΔV in (51) and J in (53) note that by (46) and (49)

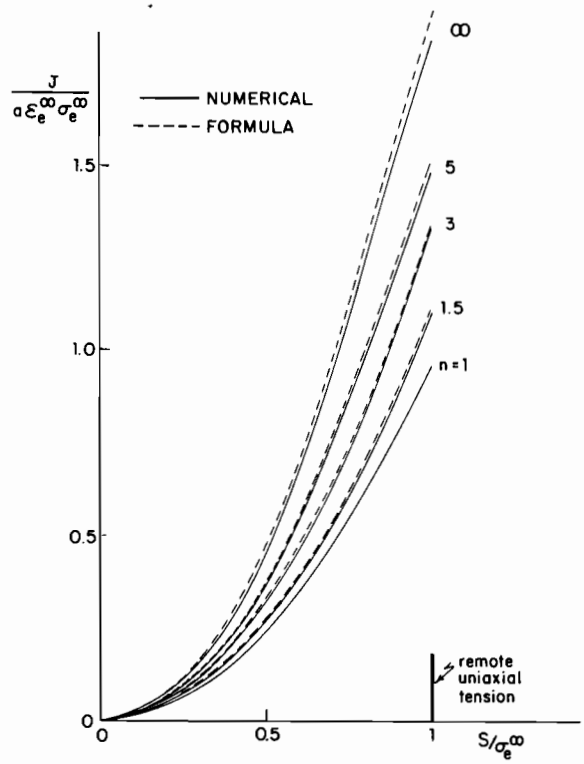

Fig. 9 Comparison between analytical results (65) and numerical results for penny-shaped crack

$$\frac{\dot{\sigma}^{\infty}}{\mu} = 3\epsilon_e^{\infty}\frac{\dot{\sigma}^{\infty}}{\sigma_e^{\infty}} = 3\epsilon_e^{\infty}\frac{S}{\sigma_e^{\infty}} \tag{63}$$

Equations (51) and (53) can therefore be written as

$$\frac{\Delta V}{\epsilon_e^{\infty} a^3} = 8\left(1 + \frac{3}{n}\right)^{-1/2}\frac{S}{\sigma_e^{\infty}} \tag{64}$$

and

$$\frac{J}{\sigma_e^{\infty}\epsilon_e^{\infty} a} = \frac{6}{\pi}\left(1 + \frac{3}{n}\right)^{-1/2}\left(\frac{S}{\sigma_e^{\infty}}\right)^2 \tag{65}$$

In applying these formulas we will take σ_e^{∞} as $|S - T|$ rather than $|T|$ since the difference in doing so involves terms of order $(\dot{\sigma}^{\infty})^3$ which have already been neglected. With $\sigma_e^{\infty} = |S - T|$ and ϵ_e^{∞} obtained from σ_e^{∞} by (1), (64) and (65) are exact for all S and T when $n = 1$. For $n \neq 1$, the error in (64) is of order $(S/\sigma_e^{\infty})^3$ since $\Delta V/\epsilon_e^{\infty}$ is odd in S/σ_e^{∞}; and, similarly, the error in J given by (65) is of order $(S/\sigma_e^{\infty})^4$.

The prediction of (64) is compared with the numerical results for h_2 from Table 1 in Fig. 8 for S/σ_e^{∞} ranging from 0 to 2. A comparison of (65) with the numerical results for h_1 is shown in Fig. 9. For remote uniaxial tension (64) and (65) become

$$\frac{\Delta V}{\epsilon_e^{\infty} a^3} = 8\left(1 + \frac{3}{n}\right)^{-1/2} \tag{66}$$

and

$$\frac{J}{\sigma_e^{\infty}\epsilon_e^{\infty} a} = \frac{6}{\pi}\left(1 + \frac{3}{n}\right)^{-1/2} \tag{67}$$

and these are compared with the most accurate set of numerical results (with $N = 3$ and $M = 3$) in Fig. 10. Equation (67) exceeds the numerical results by less than 5 percent, with the greatest difference occurring for the rigid-perfectly plastic limit. Furthermore, it is conceivable that (67) is even more accurate than Fig. 10 suggests since the numerical results give a lower bound curve.

Plane Strain Crack. The perturbation solution of the plane strain problem proceeds along similar lines so only the main results will be given. There is, however, an important mathematical difference

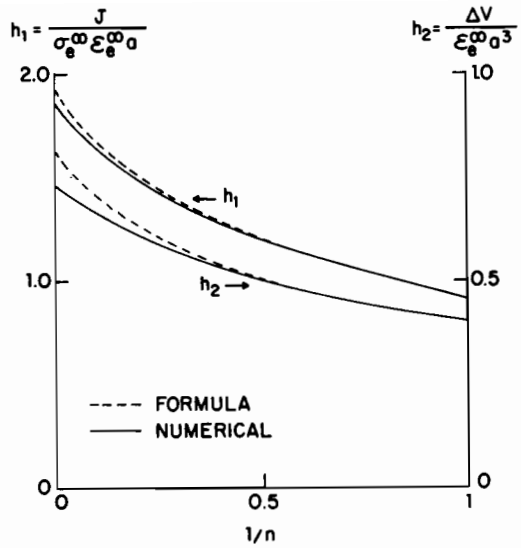

Fig. 10 Comparison of analytical results (66) and (67) with numerical results for penny-shaped crack under remote uniaxial tension ($S > 0$, $T = 0$)

between the two problems which is brought out very nicely by the perturbation solutions and this will be discussed.

The trivial state is now $\sigma_{11} = T < 0$, $\sigma_{22} = 0$, and $\sigma_{33} = T/2$ with $\sigma_e = \sqrt{3}|T|/2$ and

$$\epsilon_{22} = -\epsilon_{11} = \sqrt{3}\epsilon_e/2, \quad \epsilon_{33} = 0 \tag{68}$$

where ϵ_e is given in terms of σ_e by (1). An increment of remote plane strain tension $\sigma_{22} \equiv S = \dot{\sigma}^\infty$ is superimposed onto the trivial state. The results for this incremental problem are listed in the order developed for the penny-shaped crack in the following.

Equations (50), (51), and (53) are replaced by

$$\delta(x_1) = c(\dot{\sigma}^\infty/\mu)(a^2 - x_1^2)^{1/2} \tag{69}$$

$$\Delta A = \frac{\pi}{2} c(\dot{\sigma}^\infty/\mu)a^2 \tag{70}$$

$$J = \frac{\pi c}{4\mu}(\dot{\sigma}^\infty)^2 a \tag{71}$$

where ΔA is the area of the opened crack and μ is again given by (49). Equations (55) and (56) still hold in plane strain; and, by comparing (71) and (56), we see that $k = \sqrt{\pi}$ for all n.

In terms of the stream function $\psi(x_1, x_2)$ with $\dot{u}_1 = \psi_{,2}$ and $\dot{u}_2 = -\psi_{,1}$, equation (57) is replaced by

$$\psi_{,1111} + \left(\frac{4}{n} - 2\right)\psi_{,1122} + \psi_{,2222} = 0 \tag{72}$$

with boundary conditions

$$\left.\begin{aligned} \psi_{,11} - \psi_{,22} &= 0 \\ (4-n)\psi_{,112} + n\psi_{,222} &= 0 \end{aligned}\right\} (|x_1| < a, x_2 = \pm 0) \tag{73}$$

With $\xi = x_1 - a$, the singularity analysis gives

$$\dot{\sigma}_{22} = A\xi^{-1/2} \quad (\xi > 0, x_2 = 0) \tag{74}$$

and

$$\delta = \frac{2}{\mu}\sqrt{n}\, A(-\xi)^{1/2} \quad (\xi < 0) \tag{75}$$

Comparing (74) and (75) with (38) and (69), we find

$$c = \sqrt{n} \tag{76}$$

By (63), (70), and (71) become

$$\frac{\Delta A}{\epsilon_e^\infty a^2} = \frac{3\pi\sqrt{n}}{2}\frac{S}{\sigma_e^\infty} \tag{77}$$

and

$$\frac{J}{\sigma_e^\infty \epsilon_e^\infty a} = \frac{3\pi\sqrt{n}}{4}\left(\frac{S}{\sigma_e^\infty}\right)^2 \tag{78}$$

These formulas are again exact for all S and T when $n = 1$ if σ_e^∞ is taken as $\sqrt{3}|S - T|/2$ and ϵ_e^∞ is obtained from (1).

The solutions to the axisymmetric incremental problem are well behaved as $n \to \infty$. The governing equations (e.g., (57)) remain elliptic in this limit. In contrast, the normalized results for ΔA and J in plane strain, (77) and (78), are unbounded as $n \to \infty$ and this is associated with the loss of ellipticity of (72) in this limit. These behaviors mirror the corresponding behaviors in the rigid-perfectly plastic limit of the fully nonlinear problems. That is, the axisymmetric problem for $n \to \infty$ remains elliptic and well behaved, while the plane strain problem becomes hyperbolic admitting the possibility of discontinuous displacements and/or displacement gradients.

5 Numerical Solution for Plane Strain Crack

The numerical solution for the plane strain problem parallels that given in Section 3 for the penny-shaped crack. In fact, it is simpler to choose a representation for the stream function in the plane problem. On the other hand, the plane strain problem is ill-behaved as $n \to \infty$, as already discussed, and this makes it more difficult to generate accurate results for large n. In the axisymmetric problem it was possible to carry out calculations using the minimum principle with $n = \infty$. The plane strain solution does not obey the admissibility conditions associated with the minimum principle when $n = \infty$.

The geometry of the problem is shown in Fig. 1(*b*) and the mapping function (31) is again employed to map the slit plane onto the interior of the unit circle in the ζ-plane as in Fig. 2. Incompressibility implies the existence of a stream function ψ such that the additional displacements are given by

$$\tilde{u}_1 = \psi_{,2} \quad \text{and} \quad \tilde{u}_2 = -\psi_{,1} \tag{79}$$

In terms of the coordinates μ and ϕ in the mapping plane (see Fig. 2), ψ is taken as

$$\psi(\mu, \phi) = \sum_{k=1}^{N}\sum_{j=1}^{M} A_{kj}[\mu^{j-1}\sin 2k\phi - (-1)^k 2k(\phi - \pi/2)] \tag{80}$$

where the A's are free parameters chosen to minimize Φ. This choice meets the required symmetry of the solution with respect to the two Cartesian coordinate axes. The crack opening from (80) is of the form $f(x)\sqrt{a^2 - x_1^2}$ where $f(a)$ is bounded, and therefore (80) can only approximate the solution when $n \neq 1$.

The second term in (13) is

$$-\int_S \sigma_{ij}^\infty n_j \tilde{u}_i dS = 4\pi S \sum_{k=1}^{N}\sum_{j=1}^{M} k(-1)^k A_{kj} \tag{81}$$

The effective strain is computed using

$$\epsilon_e^2 = \frac{2}{3}\epsilon_{ij}\epsilon_{ij} = \frac{4}{3}\left[(\psi_{,12} - \epsilon_{11}^\infty)^2 + \frac{1}{4}(\psi_{,11} - \psi_{,22})^2\right] \tag{82}$$

and otherwise the numerical procedure is similar to that described

Table 3 h_1, h_2, and h_3 for plane strain crack

	S/σ_e^∞	S/T	n = 1	n = 1.5	n = 2.0	n = 3.0	n = 5.0
$h_1 = \frac{J}{a\sigma_e^\infty\epsilon_e^\infty}$	$2/\sqrt{3}$	∞	3.142	3.851	4.448	5.422	6.754
	$1/\sqrt{3}$	-1.0	0.7853	0.9591	1.100	1.333	1.639
	$4/\sqrt{3}$	2.0	12.57	15.44	17.73	22.12	27.16
$h_2 = \frac{\Delta A}{a\epsilon_e^\infty}$	$2/\sqrt{3}$	∞	5.441	6.686	7.757	9.523	11.86
	$1/\sqrt{3}$	-1.0	2.721	3.325	3.819	4.657	5.521
	$4/\sqrt{3}$	2.0	10.88	13.62	15.81	19.68	24.56
$h_3 = \frac{\delta}{a\epsilon_e^\infty}$	$2/\sqrt{3}$	∞	3.463	4.116	4.650	5.491	6.610
	$1/\sqrt{3}$	-1.0	1.732	2.095	2.391	2.854	3.340
	$4/\sqrt{3}$	2.0	6.926	8.124	9.002	10.63	12.87

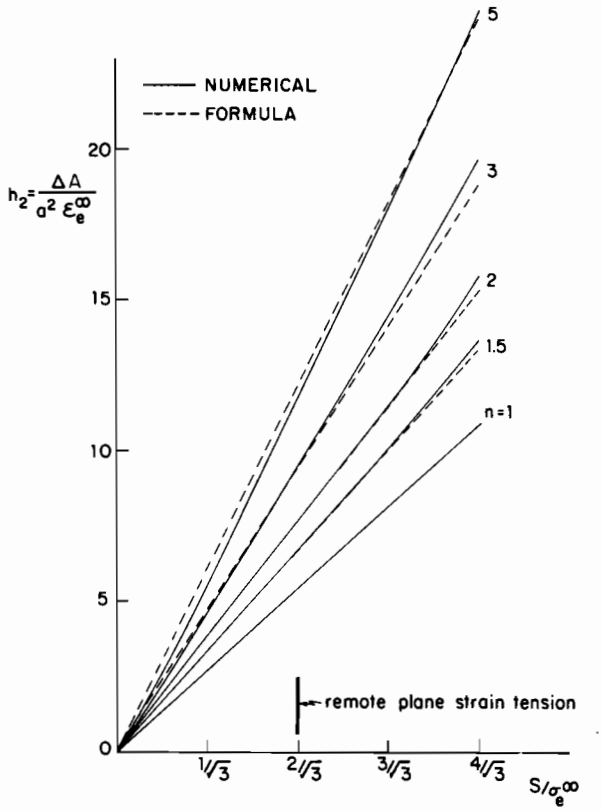

Fig. 11 Normalized crack opening area for plane strain crack; dashed line curves from (77)

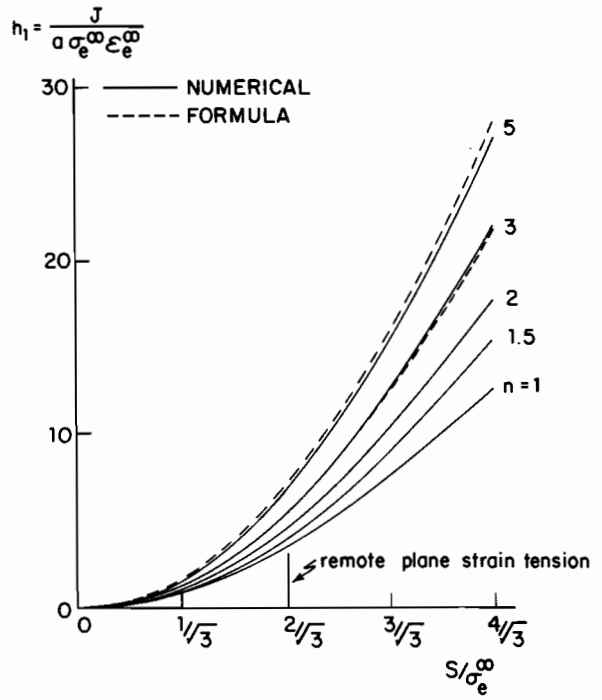

Fig. 12 Normalized J for plane strain crack; dashed line curve from (78)

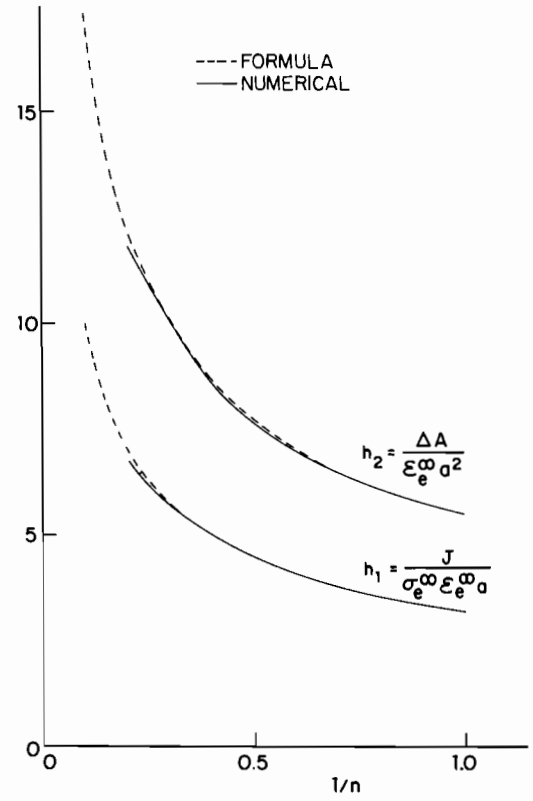

Fig. 13 Comparison between numerical results and analytical results (85) for plane strain crack in plane strain tension

for the axisymmetric problem. It can be shown that the decay of the additional displacements for large r satisfies the conditions required for application of the minimum principle as long as n is finite.

On the basis of numerical experimentation with different N and M, it is felt that the calculations with $N = 3$ and $M = 3$ give results for J in Table 3 which are low by not more than about 5 percent for $n < 3$. With $N = 3$ and $M = 4$, the same level of accuracy appears to be achieved for $n = 3$ and 5. For n larger than 5 the strain concentrates in rather narrow bands emanating from the tips, and it is not expected that our numerical method can accurately represent the solution unless many more terms are included in (82). The numerical results in Table 3 are for h_1, h_2, and h_3 which are defined by

$$\frac{J}{\sigma_e^\infty \epsilon_e^\infty a} = h_1\left(n, \frac{S}{T}\right)$$
$$\frac{\Delta A}{\epsilon_e^\infty a^2} = h_2\left(n, \frac{S}{T}\right) \tag{83}$$
$$\frac{\delta}{\epsilon_e^\infty a} = h_3\left(n, \frac{S}{T}\right)$$

where $\delta = u_2(0, 0^+), -u_2(0, 0^-)$, $\sigma_e^\infty = \sqrt{3}|S - T|/2$, and ϵ_e^∞ is related to σ_e^∞ by (1). In plane strain $\sigma_{33}^\infty = (\sigma_{11}^\infty + \sigma_{22}^\infty)/2$, $\sigma_m^\infty \equiv \sigma_{kk}^\infty/3 = (S + T)/2$ and, for $S - T > 0$,

$$\frac{S}{\sigma_e^\infty} = \frac{2}{\sqrt{3}}\left(\frac{\sigma_m^\infty}{\sigma_e^\infty} + \frac{1}{2}\right) \tag{84}$$

Curves of h_1 and h_2 as functions of S/σ_e^∞ are shown in Figs. 11 and 12 where the dashed curves are obtained from formulas (77) and (78) and the solid curves are from Table 3. For $n \leq 5$ at least, it appears that the formulas will be sufficiently accurate for many purposes for $\sigma_m^\infty/\sigma_e^\infty$ as large as $\frac{3}{2}$. Fig. 13 displays the results as plots against $1/n$ for plane strain tension ($S > 0$, $T = 0$) for which (77) and (78) become simply

$$\frac{\Delta A}{\epsilon_e^\infty a^2} = \pi\sqrt{3n} \quad \text{and} \quad \frac{J}{\sigma_e^\infty \epsilon_e^\infty a} = \pi\sqrt{n} \tag{85}$$

The relationship between (85) and those of [4] for a crack of length $2a$ in an infinite strip of width $2b$ subject to remote plane strain tension ($S > 0$, $T = 0$) is displayed in Fig. 14. In the present notation, the function h_1 of [4] is defined as

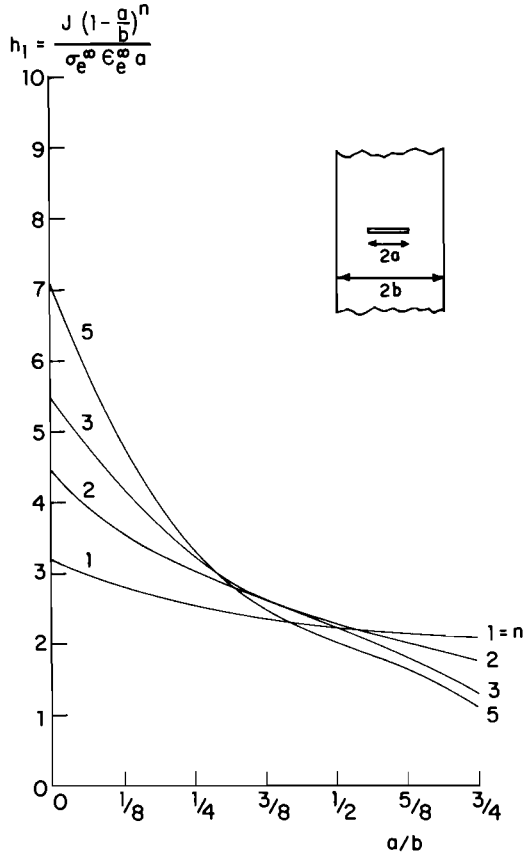

Fig. 14 Normalized J for plane strain center-cracked strip subject to plane strain tension; values for $a/b = 0$ from (85) and for $a/b > 0$ from [4]

$$h_1\left(\frac{a}{b}, n\right) = \frac{J}{\sigma_e^\infty \epsilon_e^\infty a}\left(1-\frac{a}{b}\right)^n \tag{86}$$

which coincides with the present definition of h_1 in plane strain tension when $a/b = 0$. It is seen that $h_1(a/b, n)$ is a strong function of a/b when a/b is small and $n \neq 1$. Some care should be exercised in using the results for the infinite geometry to model the finite geometry and vice versa.

Finally, contours of constant effective strain are shown in Fig. 15 for plane strain tension with $\epsilon_e^\infty = 1$ for $n = 5$. A comparison of this figure with the corresponding plot for the penny-shaped crack in Fig. 6 reveals the substantially larger strain concentration in the plane strain problem at a given distance from the crack tip. In addition, it is noted that there is a large dead zone directly above and below the center of the plane strain crack in which the effective strain is almost zero.

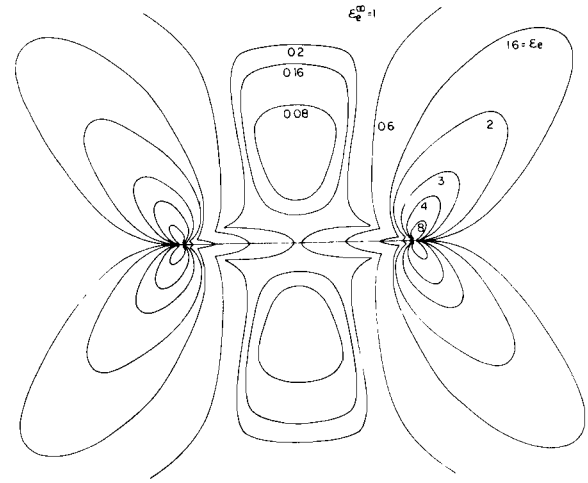

Fig. 15 Contours of constant effective strain ϵ_e for the plane strain crack subject to remote plane strain tension with $\epsilon_e^\infty = 1$ and $n = 5$

Acknowledgment

The work of M.Y.H. was supported in part by the Chinese Academy of Sciences and by the National Science Foundation under Grant ENG-78-10756. The work of J.W.H. was supported in part by the National Science Foundation under Grants DMR-79-23597 and ENG-78-10756, and by the Division of Applied Sciences, Harvard University.

References

1 Goldman, N. L., and Hutchinson, J. W., "Fully Plastic Crack Problems: The Center-Cracked Strip Under Plane Strain," *International Journal of Solids and Structures*, Vol. 11, 1975, pp. 575–591.

2 Amazigo, J. C., "Fully Plastic Center-Cracked Strip Under Antiplane Shear," *International Journal of Solids and Structures*, Vol. 11, 1975, pp. 1291–1299.

3 Ranaweera, M. P., and Leckie, F. A., "The Use of Optimization Techniques in the Analysis of Cracked Members by the Finite-Element Displacement and Stress Methods," *Computer Methods in Applied Mechanics and Engineering*, Vol. 19, 1979, pp. 367–389.

4 Kumar, V., Shih, C. F., and German, M. D., *The Handbook for Elastic-Plastic Fracture Analysis*, in preparation by the General Electric Company.

5 Shih, C. F., "J-Integral Estimates for Strain-Hardening Materials in Antiplane Shear Using Fully Plastic Solutions," in *Mechanics of Crack Growth*, ASTM STP 590, 1976, pp. 3–22.

6 Shih, C. F., and Hutchinson, J. W., "Fully Plastic Solutions and Large-Scale Yielding Estimates for Plane Stress Crack Problems," ASME *Journal of Engineering Materials and Technology*, Vol. 98, 1976, pp. 289–295.

7 Hill, R. and Storåkers, B., "Plasticity and Creep of Pressurized Membranes: A New Look at the Small-Deflection Theory," *Journal of Mechanics and Physics of Solids*, Vol. 28, 1980, pp. 27–48.

8 Hult, J., "On the Stationarity of Stress and Strain Distributions in Creep," in *Proceedings of the International Symposium on Second-Order Effects in Elasticity, Plasticity and Fluid Dynamics*, Haifa, Pergamon Press, 1962, pp. 352–361.

9 Budiansky, B., Hutchinson, J. W., and Slutsky, S., "Void Growth and Collapse in Viscous Solids," Harvard University Report, Division of Applied Sciences, MECH-15, Feb. 1980, to be published in *Mechanics of Solids*, The Rodney Hill 60th Anniversary Volume, eds., Hopkins, H. G., and Sewell, M. J., Pergamon Press, 1981.

10 Rice, J. R., "A Path-Independent Integral and the Approximate Analysis of Strain Concentration by Notches and Cracks," ASME JOURNAL OF APPLIED MECHANICS, Vol. 35, 1968, pp. 379–386.

11 Hutchinson, J. W., "Singular Behavior at the End of a Tensile Crack in a Hardening Material," *Journal of Mechanics and Physics of Solids*, Vol. 16, 1968, p p. 13–31.

12 Rice, J. R., and Rosengren, G. F., "Plane-Strain Deformation Near a Crack Tip in a Power-Law Hardening Material," *Journal of Mechanics and Physics of Solids*, Vol. 16, 1968, pp. 1–12.

13 Knowles, J. K., and Sternberg, E., "On a Class of Conservation Laws in Linearized and Finite Elastostatics," *Archive for Rational Mechanics and Analysis*, Vol. 44, 1972, pp. 187–211.

14 Budiansky, B., and Rice, J. R., "Conservation Laws and Energy-Release Rates," ASME JOURNAL OF APPLIED MECHANICS, Vol. 40, 1973, pp. 201–203.

15 Budiansky, B., and Hutchinson, J. W., "Self-Similar Shapes and Asymptotic Dilatation-Rates for Voids in Viscous Solids," in *Proceedings of the XVth International Congress of Theoretical and Applied Mechanics* (Postprints), eds., Rimrott, F. P. J., and Tabarrok, B., North-Holland Publishing Company, Amsterdam, 1980, pp. 243–249.

16 Rice, J. R., and Tracey, D. M., "On the Ductile Enlargement of Voids in Triaxial Stress Fields," *Journal of Mechanics and Physics of Solids*, Vol. 17, 1969, pp. 201–217.

17 Hoenig, A., "The Behavior of a Flat Elliptical Crack in an Anisotropic Elastic Body," *International Journal of Solids and Structures*, Vol. 14, 1978, pp. 925–934.

18 Eshelby, J. D., "The Determination of the Elastic Field of an Ellipsoidal Inclusion, and Related Problems," *Proceedings of the Royal Society*, London, Series A, Vol. 241, 1957, pp. 376–396.

APPENDIX

Additional Strains for Axisymmetric Problem

With (x, θ, y) as radial, circumferential, and axial coordinates, the additional strains are related to ψ by

$$\epsilon_x = x^{-1}\psi_{,xy} - x^{-2}\psi_{,y}, \quad \epsilon_\theta = x^{-2}\psi_{,y}, \quad \epsilon_y = -\epsilon_x - \epsilon_\theta,$$
$$2\epsilon_{xy} = x^{-2}[x(\psi_{,yy} - \psi_{,xx}) + \psi_{,x}]$$

By change of variables to μ and ϕ

$$\psi_{,x} = \psi_{,\mu}\frac{\partial\mu}{\partial x} + \psi_{,\phi}\frac{\partial\phi}{\partial x}$$

$$\psi_{,xx} = \left[\psi_{,\mu\mu}\frac{\partial\mu}{\partial x} + \psi_{,\mu\phi}\frac{\partial\phi}{\partial x}\right]\frac{\partial\mu}{\partial x} + \psi_{,\mu}\frac{\partial^2\mu}{\partial x^2} + \left[\psi_{,\phi\mu}\frac{\partial\mu}{\partial x} + \psi_{,\phi\phi}\frac{\partial\phi}{\partial x}\right]\frac{\partial\phi}{\partial x} + \psi_{,\phi}\frac{\partial^2\phi}{\partial x^2}$$

with similar expressions for the other partial derivatives of ψ. The derivatives $\partial\mu/\partial x$ and $\partial\phi/\partial x$ are given in (33), while

$$\frac{\partial^2\mu}{\partial x^2} + i\frac{\partial^2\mu}{\partial x\partial y} = \frac{\partial\mu}{\partial x}\frac{\Omega}{|\Omega|^2} + \mu\frac{\Omega'}{|\Omega|^2\omega'} - \frac{2\mu\Omega}{|\Omega|^4}\mathrm{Re}\left[\frac{\bar{\Omega}\Omega'}{\omega'}\right]$$

$$\frac{\partial^2\mu}{\partial x\partial y} + i\frac{\partial^2\mu}{\partial y^2} = \frac{\partial\mu}{\partial y}\frac{\Omega}{|\Omega|^2} + i\frac{\mu\Omega'}{|\Omega|^2\omega'} - \frac{2\mu\Omega}{|\Omega|^4}\mathrm{Re}\left[\frac{i\bar{\Omega}\Omega'}{\omega'}\right]$$

$$\frac{\partial^2\phi}{\partial x\partial y} - i\frac{\partial^2\phi}{\partial x^2} = -\frac{\Omega'}{|\Omega|^2\omega'} + \frac{2\Omega}{|\Omega|^4}\mathrm{Re}\left[\frac{\bar{\Omega}\Omega'}{\omega'}\right]$$

$$\frac{\partial^2\phi}{\partial y^2} - i\frac{\partial^2\phi}{\partial x\partial y} = -\frac{i\Omega'}{|\Omega|^2\omega'} + \frac{2\Omega}{|\Omega|^4}\mathrm{Re}\left[\frac{i\bar{\Omega}\Omega'}{\omega'}\right]$$